remote sensing

MDPI

Communication

Effect of DEM Used for Terrain Correction on Forest Windthrow Detection Using COSMO SkyMed Data

Michele Dalponte [1,*], Daniele Marinelli [1] and Yady Tatiana Solano-Correa [2]

[1] Research and Innovation Centre, Fondazione Edmund Mach, Via E. Mach, 38098 San Michele all'Adige, Italy; daniele.marinelli@fmach.it
[2] Faculty of Engineering and Sciences, Pontificia Universidad Javeriana, Calle 18 #118–250, Cali 760031, Colombia; tatiana.solano@javerianacali.edu.co
* Correspondence: michele.dalponte@fmach.it; Tel.: +39-0461-615596

Abstract: Preprocessing Synthetic Aperture Radar (SAR) data is a crucial initial stage in leveraging SAR data for remote sensing applications. Terrain correction, both radiometric and geometric, and the detection of layover/shadow areas hold significant importance when SAR data are collected over mountainous regions. This study aims at investigating the impact of the Digital Elevation Model (DEM) used for terrain correction (radiometric and geometric) and for mapping layover/shadow areas on windthrow detection using COSMO SkyMed SAR images. The terrain correction was done using a radiometric and geometric terrain correction algorithm. Specifically, we evaluated five different DEMs: (i–ii) a digital terrain model and a digital surface model derived from airborne LiDAR flights; (iii) the ALOS Global Digital Surface Model; (iv) the Copernicus global DEM; and (v) the Shuttle Radar Topography Mission (SRTM) DEM. All five DEMs were resampled at 2 m and 30 m pixel spacing, obtaining a total of 10 DEMs. The terrain-corrected COSMO SkyMed SAR images were employed for windthrow detection in a forested area in the north of Italy. The findings revealed significant variations in windthrow detection across the ten corrections. The detailed LiDAR-derived terrain model (i.e., DTM at 2 m pixel spacing) emerged as the optimal choice for both pixel spacings considered.

Keywords: SAR; windthrow detection; preprocessing; digital elevation model; digital surface model; COSMO SkyMed

Citation: Dalponte, M.; Marinelli, D.; Solano-Correa, Y.T. Effect of DEM Used for Terrain Correction on Forest Windthrow Detection Using COSMO SkyMed Data. *Remote Sens.* **2024**, *16*, 4309. https://doi.org/10.3390/rs16224309

Academic Editors: Arturo Sanchez-Azofeifa and Brenden E. McNeil

Received: 18 September 2024
Revised: 12 November 2024
Accepted: 16 November 2024
Published: 19 November 2024

1. Introduction

Synthetic Aperture Radar (SAR) images acquired over areas with complex topography often exhibit significant distortions in the backscatter values due to the side-looking nature of SAR sensors. For instance, hills facing the SAR system typically appear brighter (with higher backscatter values) because they reflect energy back toward the sensor, while hills facing away appear darker (with lower backscatter values) because they scatter energy away from the sensor. Additionally, SAR images provided in Level 1A or 1B by the data providers (e.g., European Space Agency) also need a geometric correction to determine the correct location of each pixel with respect to the ground using a digital elevation model. Usually, the process to radiometrically correct the images with respect to the topography is called radiometric terrain correction, while the correction of the geometric distortions and the correct positioning of the pixels with respect to the terrain is called geometric terrain correction.

SAR images in complex topography can be affected by layover and shadows. Layover occurs when the radar beam reaches the top of a tall feature before reaching its base. In a SAR image with layover, the mountains look as if they have fallen over toward the sensor. Steeper angles lead to more extreme layovers, where mountain tops appear to lay over their base. Layover pixels appear to have high values in the image (bright pixels).

Shadows in SAR images arise when higher objects obstruct the radar beam, resulting in certain areas not being illuminated and appearing dark due to the absence of backscattered energy. The extent of shadow effects increases as the radar beam's incidence angle becomes more oblique with respect to the surface. Where slopes are very steep, the dim side may be completely dark because no radar signal is returned at all. Before SAR images can be reliably used for surface mapping and change detection, it is essential to correct the backscatter values for topographic effects and to address distortions caused by layovers and shadows. The process adopted to map layover and/or shadow areas is known as layover/shadows masking.

Many algorithms exist in the literature to perform both radiometric and geometric terrain correction [1–4] and layover/shadows masking [5–8] and all of them rely on the use of a Digital Elevation Model (DEM). A DEM is the umbrella term to indicate, in the most generic possible way, an elevation model. Inside DEMs it is possible to differentiate two products, the digital terrain models (DTMs) and the digital surface models (DSMs). A DSM is the specific term to indicate a surface model, i.e., it represents the absolute elevation at the very top of solid objects in the scene; it includes buildings, infrastructures, and vegetation. A DSM is therefore a DEM, but a DEM is not necessarily a DSM. A DTM is the specific term to indicate the elevation of the natural topography, i.e., after having removed vegetation and man-made buildings. As for the DSM, a DTM is a DEM, but a DEM is not necessarily a DTM. There are some worldwide DEMs that are widely used for remote sensing applications, such as the SRTM [9], the ASTER [10], the ALOS [11], or the Copernicus one [12]. These models are usually DSMs, or if based on SAR data, they could be either a DSM, a DTM, or something in between depending on the SAR wavelength. Such data are available worldwide, but they typically have a significantly coarser pixel spacing compared to those generated from LiDAR data. Airborne LiDAR-based DEMs are available nationwide in a few countries or locally in some regions of the world.

Terrain correction with a detailed VHR DEM becomes particularly important when using SAR data at a VHR. Indeed, the most advanced and recent satellite constellations acquire SAR images with a pixel spacing in the order of meters or even sub-meters (VHR). In these cases, the terrain correction with a high-spatial-resolution model becomes fundamental to preserving the spatial details of the images [13,14]. According to the CEOS recommendations [15], in order to topographically correct SAR images, the DEM should have a spatial resolution as good or better than the spatial resolution of the image to correct. This means that, optimally, to correct VHR SAR images, it is necessary to have a VHR DEM.

Thus, the aim of this study is to evaluate the effect of DEM on terrain correction and layover/shadows mapping of VHR SAR images. These are fundamental steps in SAR data processing, and thus, a correct understanding of the most suitable DEM to use is very important for many applications. We considered VHR images acquired with the COSMO SkyMed constellation over an area located in the north of Italy. SAR images could be used in many types of applications; to evaluate the effect of the DEM also on a real application in this study, we decided to focus on change detection, in particular on windthrow detection. SAR images have been used successfully for this application previously in many studies [16,17] and using VHR SAR images [18]. While windthrow detection is but one potential application of SAR data for change detection, its importance is expected to grow in response to forecasts of increased windthrow events due to global warming [19]. SAR data, with its ability to penetrate cloud cover, could emerge as a valuable tool for mapping damages resulting from such events.

2. Materials and Methods

2.1. Materials

2.1.1. Study Area and Reference Data

The study area is the North-Eastern part of the Autonomous Province of Trento (PAT) in Italy (see Figure 1). Characterised by predominantly mountainous terrain, the landscape is dominated by tree species such as Norway spruce (*Picea abies* (L.) H. Karst), silver fir

(*Abies alba* Mill.), and European beech (*Fagus sylvatica* L.). In late October 2018, the entire Northeastern region of Italy, including the study area, was struck by the devastating Vaia storm, one of the most severe storm events witnessed in Italy in recent decades [20]. This storm had devastating effects on the forests of Northern Italy and of the Autonomous Province of Trento in particular [21].

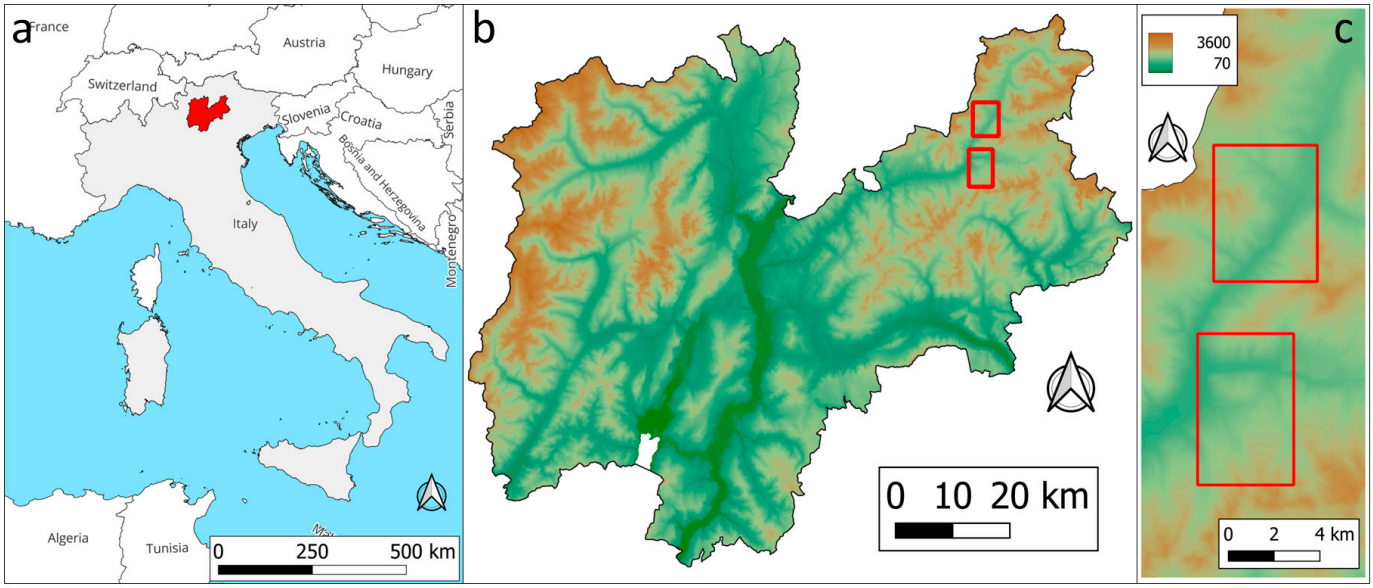

Figure 1. The location of PAT in Italy and Europe (inset (**a**)), the location of the two reference sites inside the territory of PAT and the DTM of PAT (inset (**b**)), and the DTM of the two reference areas A and B (inset (**c**)).

Reference data used for windthrow detection were established in two distinct sites of about 27 km^2 each (Figure 1, Table 1). These sites were previously examined in a separate study, with further details available in [18] (areas A and B of the study in [18]). The reference windthrow maps were established through manual photointerpretation using VHR imagery (i.e., SPOT5 images) [18]. Given the absence of relevant differences between the two sites, in this analysis they were treated as a single site.

Table 1. Characteristics of the two study areas.

		A	B
Area (km^2)	Non-forest	6.1	3.9
	Intact forest	16.3	20.9
	Windthrows	5.0	3.1
	Total	27.4	27.9
Windthrows patches	Number	456	774
	Area range (m^2)	36–1,746,189	9–389,781
	Median area (m^2)	472.5	288
Altitude a.s.l. (m)	Range	1095–2318	989–2291
	Median	1513	1511
Slope (°)	Range	0.003–77.7	0.009–79.2
	Median	29.7	24.9
Aspect (°)	Range	0–360	0–360
	Median	154.8	233.8
Forest Types (%)	Deciduous	12.2	5.4
	Evergreen	87.8	94.6

2.1.2. SAR Data

COSMO SkyMed, managed by the Italian Space Agency (ASI), is a SAR satellite constellation with four medium-sized satellites. It offers global coverage and can revisit areas of interest twice daily, regardless of weather conditions. The SAR data, available in X-band and single- or dual-polarisation modes, have varying spatial resolutions based on acquisition modes, and they are acquired on demand. For this study, two pre-event and two post-event images acquired in Stripmap HIMAGE mode with HH polarisation were used (ascending and descending, Table 2). ASI provided the images in processing level 1B—Detected Ground Multi-look (DGM), with a range and azimuth resolution of 5 meters, pixel spacing of 2.5 m, and swath width and scene length of 40 km. The equivalent number of looks is slightly greater than 3 for all images.

Table 2. COSMO SkyMed images used in this study.

Direction	Time	Date	Incidence Angle
Ascending	Pre-event	16 August 2018	26.5°–27.1°
	Post-event	3 August 2019	26.5°–27.1°
Descending	Pre-event	9 August 2018	31.4°–31.9°
	Post-event	23 August 2019	31.4°–31.9°

2.1.3. Digital Elevation Models

We considered five different DEM models for this study (Table 3): (i) DTM: a local DTM extracted from a LiDAR flight released in 2020 [22]; (ii) DSM: a local DSM extracted from a LiDAR flight released in 2020 [23]; (iii) ALOS: the ALOS Global Digital Surface Model released in 2021 (version 3.2) [11]; (iv) COP: the Copernicus global DEM released in 2019 [12]; and (v) SRTM: the Shuttle Radar Topography Mission (SRTM) released in 2003. The pixel spacing of each DEM model is detailed in Table 3. It is worth noting that for the global DEM, the native pixel spacing was in degrees (1 arcsecond), and they were all reprojected in the local reference system in meters (i.e., EPSG 25832). Thus, the pixel spacing in meters reported in Table 3 are the ones after reprojection to the common system.

Table 3. DEM characteristics.

DEM	Origin	Data Acquisition Year(s)	Pixel Spacing (m)
DTM	Airborne LiDAR data	2014–2018	0.5
DSM	Airborne LiDAR data	2014–2018	0.5
ALOS	Stereo optical data	2006–2011	~26.5
COP	Band-X SAR data	2011–2015	~23.7
SRTM	Band-C SAR data	2000	~26.5

The three global DEMs (i.e., ALOS, COP, and SRTM) are generated from three different sources. ALOS is generated starting from the Panchromatic Remote-sensing Instrument for Stereo Mapping (PRISM), which was a panchromatic radiometer with 2.5 m spatial resolution at nadir. The objective of PRISM was to obtain high-resolution stereo data (pixel size of 2.5 m) for cartographic applications (extraction of highly accurate digital elevation models, etc.). Thus, ALOS DEMs are based on optical stereo data at high resolution. COP and SRTM DEMs are based on SAR data. COP is generated from the TanDEM-X SAR images acquired in band X, while SRTM is generated from C-band SAR data. The five DEMs were upsampled/downsampled using bilinear interpolation to a pixel spacing of 2 m and 30 m, and the upsampled/downsampled DEMs were used in the elaborations.

2.2. Methods

The methods adopted in this study are summarised in Figure 2, where the same process is carried out for different DEMs, ending up with several windthrow detection results that allow us to compare the impacts of using different DEMs for the terrain correction process. In the next paragraphs, each step is detailed.

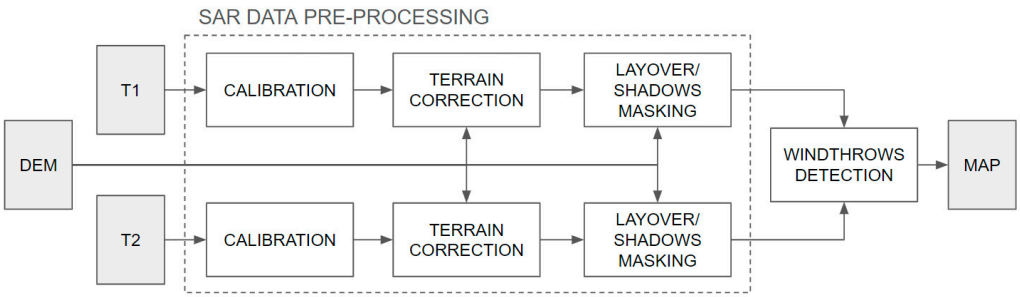

Figure 2. Architecture of the processing chain adopted in this study.

2.2.1. Calibration

The COSMO SkyMed SAR calibration was carried out using the calibration module (https://step.esa.int/main/wp-content/help/versions/10.0.0/snap-toolboxes/eu.esa.microwavetbx.sar.op.calibration.ui/operators/CalibrationOp.html, accessed on 15 November 2024) implemented in the SNAP software (SNAP—ESA Sentinel Application Platform v8.0, http://step.esa.int, accessed on 15 November 2024). This module is designed to convert the raw digital numbers (DNs) of SAR data into backscatter intensity. Calibration is important because it helps make the data more accurate, meaningful, and consistent across different times and locations. Specifically, the calibration module converts the DNs of the Level 1B images into backscatter coefficients, which represent the normalised radar cross-section of the surface. The backscatter coefficients could be sigma0, beta0, and gamma0. Sigma0 represents the radar reflectivity per unit area on the ground, normalised by the cosine of the incidence angle; beta0 represents the radar brightness, which is the backscatter per unit area in the radar slant range plane; and gamma0 is similar to sigma0 but normalised by the cosine of the local incidence angle, which accounts for variations in terrain slope. Moreover, the calibration module corrects for instrumental and environmental factors: the calibration corrects for the effects of the instrument's characteristics and environmental conditions to provide a more consistent and standardised measurement. This includes correcting for differences in the radar's look angle, range distance, and power variations.

2.2.2. Terrain Correction

Other than the calibration itself, SAR data needs to be corrected for distortions that are mainly related to side-looking geometry. Thus, terrain corrections aim at ensuring that such distortions will be corrected and the resulting image will be as close as possible to the real world. Even though methods can be found in literature that can help to reduce the above-mentioned distortions [1–3,24,25], they are all based on similar principles. Given this, in this work we decided to make use of one of the most used methods in literature, being the one offered by ESA on their SNAP platform for processing Sentinel data (SNAP—ESA Sentinel Application Platform v8.0, http://step.esa.int, accessed on 15 November 2024). The terrain correction step is made up of two main steps: (i) radiometric terrain correction (TF) and (ii) geometric terrain correction (TC). In this study, both steps were applied using state-of-the-art methods implemented in the software SNAP. Inside the SNAP modules, when requested, a bilinear interpolation was used.

The radiometric terrain correction was done using the terrain flattening module of SNAP that is implementing the radiometric terrain correction algorithm proposed by Small [26]. The algorithm using a DEM, resampled to a pixel spacing equal to or better than

the one of the SAR data, normalises the backscatter with respect to the local incidence angle, effectively reducing the influence of slope and topographic effects on the measured signal.

The geometric terrain correction was done using the range-doppler terrain correction module of SNAP that applies the method proposed in [27] for geocoding SAR images from single 2D raster radar geometry. The algorithm uses a DEM to accurately model and compensate for distortions due to topography, ensuring that each pixel in the SAR image is correctly geolocated. The module applies the range-Doppler equation, which relates the sensor's range and Doppler history to the ground coordinates, in combination with the DEM to project the slant-range image into a ground-range, map-projected coordinate system.

Additionally, in these two steps, during the terrain correction, it is also important to map and mask the layover/shadow areas. In this study, this was done using the algorithm presented in [27] that we implemented in an R [28] script. This algorithm uses as input the DEM, the SAR incidence angle with respect to the ellipsoid, and the SAR local incidence angle. These last two products were obtained as output of the range-doppler terrain correction module.

2.2.3. Windthrow Detection Algorithm

The windthrow detection methodology used was developed starting from the one proposed by [29] to detect forest fires using ERS-1 SAR data. The algorithm takes in input one pre- and one post-event SAR image already pre-processed with the terrain correction. The strength of this method is that it decomposes the images at different scales. The algorithm has been successfully used in previous studies [18], and we refer the reader to [18,29,30] for a detailed description of it.

The algorithm is organised into four steps: (i) creation of the log ratio image: the logarithm of the ratio between the pre-event image and the post-event image in linear scale. The ratio is used instead of the difference due to speckle noise present in these images: the statistical distribution of the data changes and cannot be compared by standard subtraction; (ii) multiscale decomposition/reconstruction: this step is done using a 2D stationary wavelet transform (2D-SWT) using a Daubechies filter of 8. As windthrow in each area have different sizes, they cannot be compared on the same scale, otherwise smaller or larger windthrows would be missed (iii) Otsu thresholding of each multiscale component: given the analysis at different scales, separate thresholds are required in order to improve detection capability; and (iv) final decision using a majority rule for each pixel: a given pixel could be observed more than once at different scales, reporting different results, thus a majority rule helps to assign the best label. Afterwards, an additional spatial filtering of 3×3 pixels based on a majority rule is applied to the final map.

In the case of the use of both ascending and descending images, the algorithm could be applied either to the mosaic or to each couple separately, and the windthrow maps merged. In this study we decided to use this second option: any pixel detected as windthrow in the ascending and/or descending map was considered as windthrow in the final map.

3. Results

As a first analysis, we visually compared the five DEMs at 2 and 30 m: we subtracted from four DEMs (i.e., DSM, ALOS, COP, and SRTM) the DTM obtained using LiDAR data (that we consider to be the most precise one). We considered the entire study area (Figures 3A and 4A), a small, almost flat area (Figures 3B and 4B), a small forest area (Figures 3C and 4C), and two transects (Figures 3D and 4D). As it could be seen in Figure 3A–C), subtracting the LiDAR DTM from the LiDAR DSM at 2 m pixel spacing results in the canopy height model where the crowns are quite visible (Figure 3C). When working at 30 m pixel spacing (Figure 4A), the crowns are no more visible, and the elevation value in the pixels is influenced by both the presence of the trees and by the gaps in the canopy. Subtracting the three satellite-based DEMs, the DTM generated large areas with high elevation differences (from −73 to +232 m). These differences are partially related to

the tree's coverage and partially to the topography of the area. The topographic differences are clearly highlighting small valleys and microtopography related to water catchments, or very steep areas. These are the areas where we have the highest differences between the LiDAR-based DTM and the three global DEMs. In the difference images for the three global DEMs, a kind of tiling pattern is also visible; this could be related to the fact that the five DEMs were not mutually calibrated among each other, and it could also be an issue present in the ALS-derived DTM and DSM. In Figures 3D and 4D, a comparison among the five DEMs over two transects (one South to North and one West to East) is also shown. First, the canopy of the forest is very clearly highlighted in the LiDAR-derived DSM at 2 m pixel spacing (red line in Figure 3D), while moving at 30 m pixel spacing, the LiDAR DSM becomes more like the DTM. The DTM at 2 m pixel spacing is also describing much better the microtopography that gets lost at 30 m. Additionally, it is visible that the three global DEMs are neither DTMs nor DSMs, and they are losing the microtopography due to their lower pixel spacing. The three global DEMs are not much different at 2 m and 30 m pixel spacing, as the upsampling was done with an interpolation and not through a pansharpening process. From these graphs (Figures 3D and 4D), it seems also that the COP DEM (blue line) is the closest to the LiDAR DSM among the three global DEMs considered, while ALOS (green line) seems closer to the LiDAR DTM (black line).

In Table 4, we present the percentage of pixels flagged as layovers/shadows within the two reference areas. The data are organised by image. Notably, there is a difference between the ascending and descending acquisitions, probably related to the topography of the two areas: while for the ascending images the percentage of layover/shadow pixels is around 36%, for the descending acquisitions it is much lower (around 8%). The only value that is not in line with the others is the one obtained using the LiDAR-based DSM at 2 m pixel spacing, where, for the descending images, the percentage of layover/shadow areas is much higher (about 22%).

Table 4. Percentage of pixels detected as layover/shadows inside the two reference sites for each image, varying the DEM and the pixel spacing. A = ascending image; D = descending image.

DEM	Pixel Spacing (m)	9 August 2018 (D)	16 August 2018 (A)	3 August 2019 (A)	23 August 2019 (D)
DTM	2	7.6	37.1	37.1	7.6
	30	8.9	36.3	36.3	8.9
DSM	2	22.3	33.8	33.7	22.4
	30	9.5	35.8	35.8	9.4
ALOS	2	7.2	36.5	36.6	7.1
	30	8.9	36.1	36.1	8.9
COP	2	6.8	36.2	36.3	6.8
	30	8.3	36.0	36.0	8.3
SRTM	2	6.6	36.2	36.2	6.6
	30	7.7	36.0	36.0	7.7

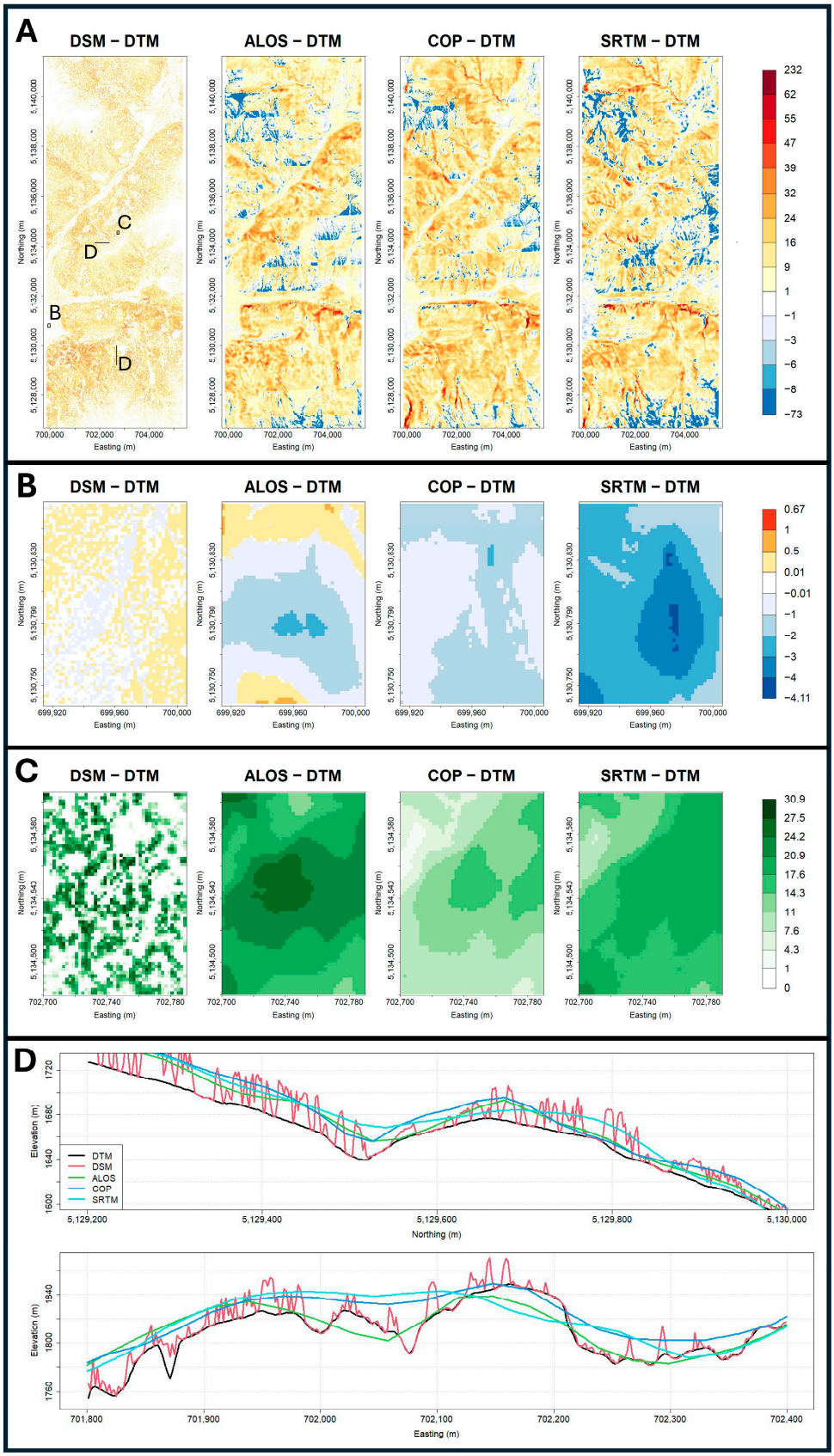

Figure 3. (**A**) Difference images at 2 m pixel spacing between the local LiDAR DSM, the three global DEMs, and the local LiDAR DTM; (**B**) a zoom over a flat area (cropland); (**C**) zoom over a forest area; and (**D**) two vertical profiles of the five DEMs at 2 m pixel spacing.

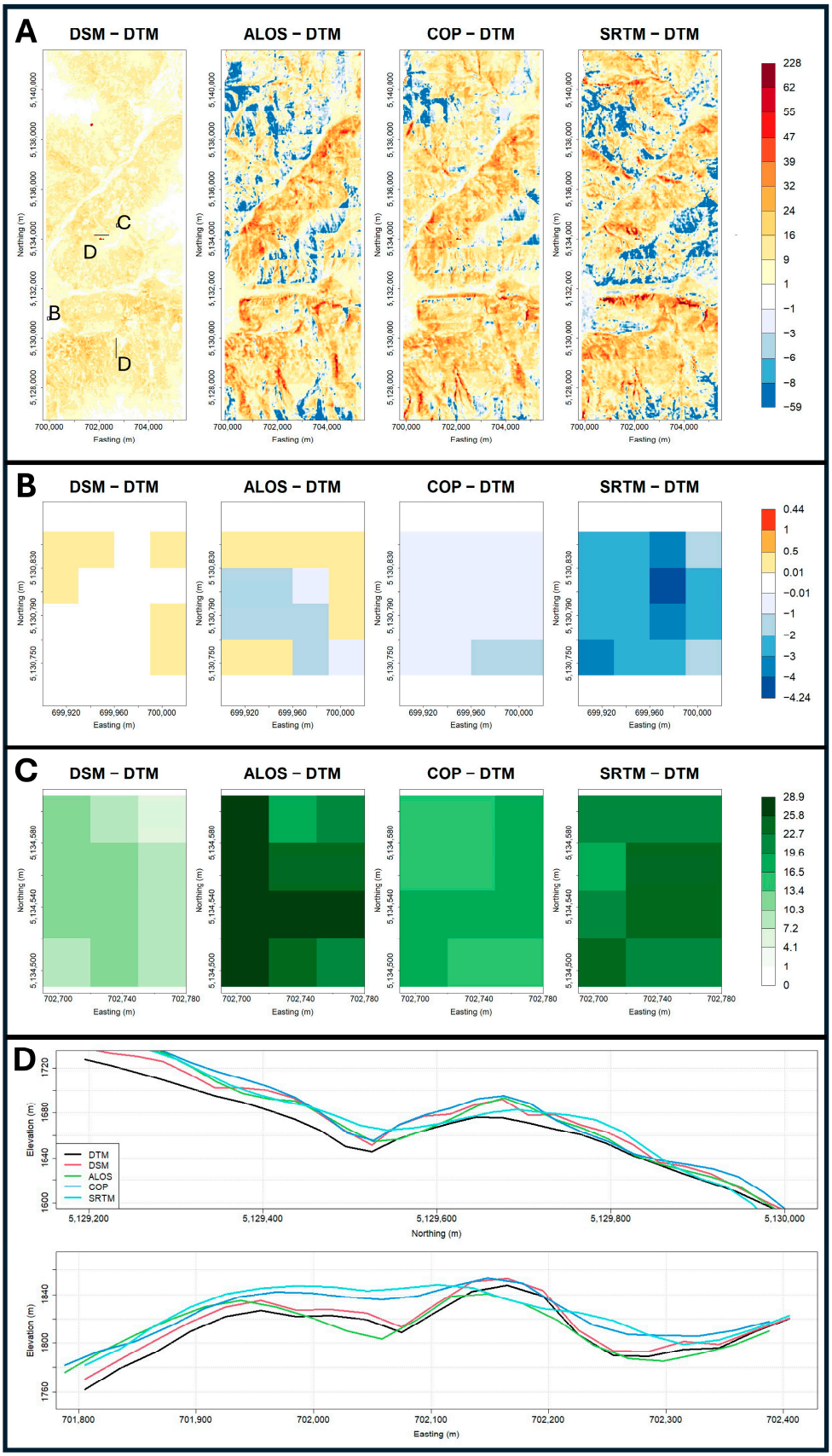

Figure 4. (**A**) Difference images at 30 m pixel spacing between the local LiDAR DSM, the three global DEMs, and the local LiDAR DTM; (**B**) a zoom over a flat area (cropland); (**C**) zoom over a forest area; and (**D**) two vertical profiles of the five DEMs at 30 m pixel spacing.

In Table 5, we present the results of windthrow detection with varying DEMs used for SAR image correction. We considered only the areas not detected as layovers/shadows for all DEMs analyzed. These results were obtained by calculating combined accuracies over the two reference areas. It is evident that the highest accuracies were achieved with images terrain-corrected with the LiDAR-derived DTM at 2 m pixel spacing (kappa accuracy around 0.53), followed by the DTM at 30 m pixel spacing (kappa accuracy around 0.48). The lowest accuracy (kappa around 0.2) was obtained by images terrain-corrected with the LiDAR-derived DSM at 2 m pixel spacing and COP DEM at 2 m pixel spacing. ALOS, COP, and SRTM at 30 m provided quite similar accuracies, ranging from values of kappa accuracy around 0.45 for ALOS and 0.41 for COP.

Table 5. Windthrow detection results in terms of kappa accuracy, balanced accuracy, producer's accuracy, and user's accuracy.

DEM	Pixel Spacing (m)	Kappa Accuracy	Balanced Accuracy (%)	Producer's Accuracies (%)		User's Accuracies (%)	
				NW	W	NW	W
DTM	2	0.532	82.3	84.6	79.9	95.3	52.0
	30	0.489	80.1	83.0	77.1	94.6	48.7
DSM	2	0.267	70.3	67.1	73.4	92.4	31.8
	30	0.473	79.1	82.6	75.6	94.2	47.7
ALOS	2	0.436	77.6	80.6	74.6	93.8	44.6
	30	0.45	78.2	81.4	75.0	94.0	45.7
COP	2	0.273	70.6	67.6	73.5	92.4	32.2
	30	0.419	76.7	80.1	73.3	93.5	43.5
SRTM	2	0.383	75.2	77.5	72.9	93.2	40.5
	30	0.437	77.3	81.2	73.4	93.6	45

Upon examination of the detection maps of the study areas shown in Figure 5, the results of Table 5 are confirmed. Additionally, it is quite clear that the use of the LiDAR-based DSM at 2 m pixel spacing creates a lot of scattered shadow areas due to the very detailed information of the tree crown shapes. ALOS, COP, and SRTM are also generating more false alarms compared to the LiDAR-based DTM (at both 2 and 30 m pixel spacing).

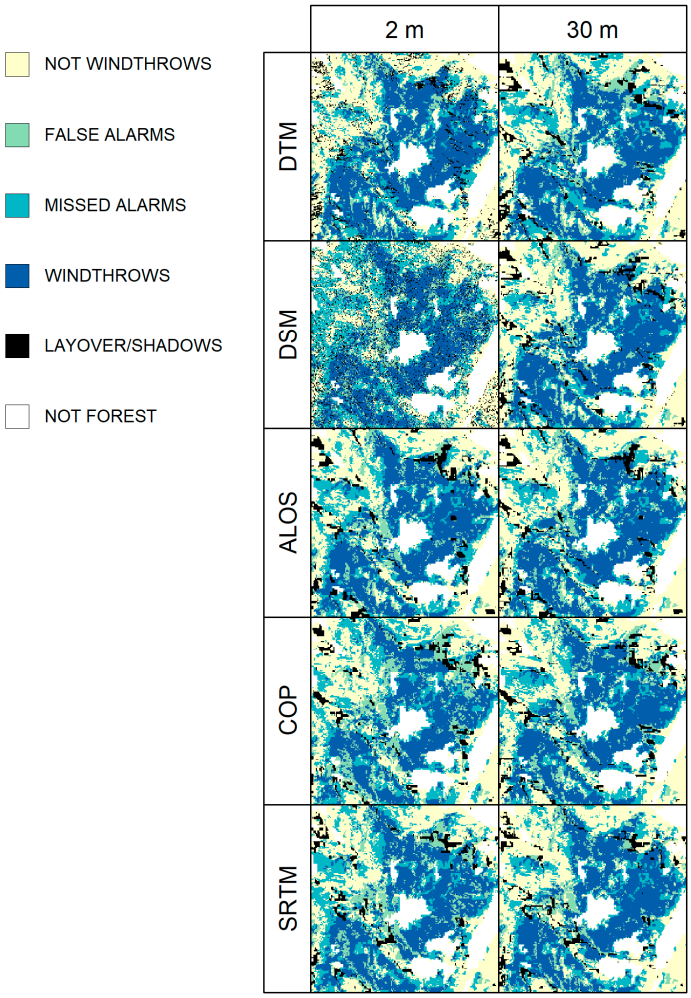

Figure 5. Windthrow detection maps for a subset of the study area.

4. Discussion

To the best of our knowledge, this study represents one of the first investigations into the impact of DEMs on terrain correction for COSMO SkyMed images. While our focus is on COSMO SkyMed data and windthrow detection, the insights gleaned from this research hold relevance for anyone involved in SAR image terrain correction.

The use of DEMs with a fine pixel spacing (i.e., 2 m) in the processing of VHR SAR images emerged to be of high importance, as underlined in [15] and [31]. In particular, in [31] the authors underlined that when the pixel spacing of DEM is too rough compared with that of SAR images, lots of spatial information on SAR images will be lost in regions where the terrain changes significantly. This is the case in mountain areas where the terrain elevation can change rapidly.

The results obtained with the LiDAR-based DTM at 2 m pixel spacing are undeniably superior to all other datasets. Even when downsampled to 30 m pixel spacing, the LiDAR DTM still provides better corrections than satellite DEMs downsampled at 30 m pixel spacing. This is probably more related to the type of information contained in the DTM itself than to the pixel spacing: while the global satellite DEMs are neither representing the terrain nor the surface (i.e., they are neither DTM nor DSMs), the LiDAR-derived DTM is representing the terrain very accurately. When subtracting the LiDAR DTM from the satellite-based DSMs, significant terrain features emerge, with height differences in the range of −73 to +232 meters. These variations have a direct impact on SAR image corrections, particularly in areas with rugged terrain, where finer topographical details improve the accuracy of the corrections. In [32], Lee et al. analysed the geolocation accuracy

of COSMO-SkyMed images corrected with a local LiDAR DTM and global DEMs, finding that LiDAR DEM consistently produced superior results across all datasets. Additionally, they observed that the commonly used global DEMs, such as SRTM and ASTER, introduced significant terrain distortions, particularly in mountainous regions.

The differences in results obtained when using the same DEM at different pixel spacings (e.g., 2 m vs. 30 m) suggest that it is preferable to use global DEMs at their native resolution. Allowing SNAP to manage any discrepancies in pixel spacing between the DEM and the SAR image yields better outcomes than manually upsampling the DEM before processing in SNAP. Indeed, the SNAP module for terrain flattening requires a DEM pixel spacing higher than the image pixel spacing, and when this is not the case (as for the 30 m pixel spacing DEMs in our study), SNAP either oversamples the DEM to higher pixel spacing or multilooks the source image to lower resolution (https://step.esa.int/main/wp-content/help/versions/10.0.0/snap-toolboxes/eu.esa.microwavetbx.sar.op.sar.processing.ui/operators/TerrainFlatteningOp.html, accessed on 15 November 2024). Choosing this second option means that the SAR image is not terrain corrected at 2.5 m using a 30 m pixel spacing DEM, but it is multi-looked to 30 m and terrain corrected at 30 m. The worst results were observed with the LiDAR-based DSM at 2 m pixel spacing. A problem could be that geolocation errors caused by the positive elevation bias of the DSM have a bigger impact at 2 m than at 30 m: residual shifts remain within the same pixel at 30 m but result in wrong pixel collocation at 2 m. Additionally, the high level of detail in crown characterisation led to numerous false layovers and shadow areas, likely caused by excessive height variations that also interfered with terrain correction. This is evident in the map of Figure 5, which shows numerous scattered regions of layover and shadow, likely due to the shadows cast by tree crowns. While using a detailed DSM can be beneficial, as it may capture canopy gaps that influence VHR SAR images, the temporal gap of 3 to 4 years between the LiDAR DSM and the imagery is problematic. Canopy gaps present in the DSM may have since been partially filled, while new gaps could have emerged, given that selective logging is routinely practiced in the study area. This temporal misalignment between the datasets could therefore be one of the reasons for the bad outcomes of this terrain correction.

Among the global DEMs, COP is the one that, if used in the SAR image corrections, is resulting in the lowest accuracy in windthrow detection. From Figures 3D and 4D, it emerged that, at least over our study area, COP is the closest to the LiDAR DSM, and on the official documentation of the COP DEM, it is specified that it is a digital surface model that represents the surface of the Earth, including buildings, infrastructure, and vegetation [12]. COP global DEM is based on Tandem-X data: InSAR-based DEMs represent the phase height corresponding to the mean scattering centre, meaning that the true surface elevation is not correctly captured over vegetation. The mean scattering centre height depends on the vegetation, the considered resolution, and the wavelength. Considering a common 30 m pixel spacing for the COP DEM and the SRTM, the only differences between these two DEMs lie in the potential vegetation difference due to the temporal separation between the products and the COSMO SkyMed acquisitions and in the use of the X- and C-band signals, respectively. In [33], InSAR tree heights predicted with Tandem-X data were compared with tree heights generated with LiDAR. The RMSE was between 0.7 and 2.3 m. Many other studies (e.g., [33,34]) exist on the use of Tandem-X data to retrieve forest canopy, and all of them highlight the fact that the penetration of Tandem-X data in the canopy is dependent also on environmental factors, and it is not always the same. Indeed, the COP DEM over vegetated areas has, in any case, lower values with respect to the LiDAR-derived DSM, so it is not properly correct to call it DSM over vegetation. Tandem-X data also has a very high spatial resolution (less than 3 m) when acquired in stripmap mode, but we expected that in the generation of the COP DEM this detail got lost.

ALOS is the global DEM that seems to provide images with the best terrain corrections to be used for windthrow detection. In [35], Chai et al. evaluated the accuracy of some global DEMs and a LiDAR DTM; in particular, they considered all three global DEMs used

in this study. From their results, it emerged that, as expected, a LiDAR DTM is the most precise in both barren land and forested areas, while among the global DEMs, ALOS seems the most accurate. On the opposite, COP DEM resulted in the least accurate. It is worth noting that in [35] they used COP DEM at 90 m.

A factor that should be considered, that is independent from the results, is also the data availability. As this study points out, and also other studies did [32], a local LiDAR DTM is the best option, but it is also the most expensive, as LiDAR data needs to be acquired if not available, and thus is frequently an option that is not viable in many parts of the world.

It is important to note that in emergency scenarios, obtaining SAR images with the same orbit and optimal imaging conditions, as utilised in this study, is often challenging. In such cases, the availability of imagery is constrained by satellite acquisition schedules, making it necessary to work with images captured from different orbits and angles. This limitation can introduce geometric distortions and variations in backscatter, which may impact the accuracy of the terrain corrections and windthrow detection. Even though this is not the main focus of this paper, the authors have addressed the reality of suboptimal conditions in emergency applications in [18]. In [18], the authors thoroughly analysed the effects of using images with varying orbits and angles, comparing optimal pre- and post-event images with suboptimal ones. The findings demonstrate that while the results are generally more accurate with optimal imagery, the proposed methods remain effective even when working with less-than-ideal data. This highlights the robustness of the approach in real-world emergency situations, where rapid response often necessitates the use of available, rather than optimal, images.

It is noteworthy that while there has been considerable attention devoted to developing algorithms for terrain correction, scarce research has delved into the influence of the DEM used for this purpose. A previous study [36] similarly noted that high-resolution DEMs contribute to higher-quality sigma0 images, underscoring the importance of DEM selection in SAR image processing. In [37] a detailed study on the preprocessing of Sentinel-1 images using the SNAP software has been done, comparing different freely available DEMs and resampling algorithms. The authors of [37] found that the DEMs affected the results, with SRTM performing better in the correction. It is worth noting that Sentinel-1 data spatial resolution is coarser compared to COSMO SkyMed.

5. Conclusions

This paper presents some insights about the impact of the DEM used for applying terrain correction on SAR data, more specifically on COSMO SkyMed SAR images. To evaluate the results, an application case was selected for windthrow detection, and five different DEMs were evaluated at different pixel spacings, 2 m and 30 m, derived from different sources. The results showed that there are significant discrepancies in windthrow detection across the five corrections. Among the five different DTMs, the local DTM at VHR (2 m pixel spacing) was the one that provided terrain-corrected images most suitable for windthrow detection, while the VHR DSM at 0.5 m pixel spacing had the worst performance. Concerning the global DEM, images corrected with ALOS DEM seem to be the ones most suitable for windthrow detection, while the ones corrected with the COP DEM are the least.

For future works, it would be interesting to not only evaluate different DEMs but also to compare them with other SAR data at lower spatial resolutions, for instance, data from Sentinel-1.

Author Contributions: Conceptualisation, M.D.; methodology, M.D., D.M. and Y.T.S.-C.; software, M.D.; validation, M.D. and D.M.; formal analysis, M.D., D.M. and Y.T.S.-C.; investigation, M.D., D.M. and Y.T.S.-C.; data curation, M.D.; writing—original draft preparation, M.D. and Y.T.S.-C.; writing—review and editing, M.D., Y.T.S.-C. and D.M.; supervision, M.D. All authors have read and agreed to the published version of the manuscript.

Funding: This research received no external funding.

Data Availability Statement: Data is not available due to the provider source.

Acknowledgments: This work was carried out using CSK® Products, © ASI (Italian Space Agency), delivered under an ASI license to use. The authors are thankful to ASI for their help with distributing the data for the different experiments.

Conflicts of Interest: The authors declare no conflicts of interest.

References

1. Flores-Anderson, A.I.; Parache, H.B.; Martin-Arias, V.; Jiménez, S.A.; Herndon, K.; Mehlich, S.; Meyer, F.J.; Agarwal, S.; Ilyushchenko, S.; Agarwal, M.; et al. Evaluating SAR Radiometric Terrain Correction Products: Analysis-Ready Data for Users. *Remote Sens.* **2023**, *15*, 5110. [CrossRef]
2. Zhao, L.; Chen, E.; Li, Z.; Fan, Y.; Xu, K. Radiometric Terrain Correction Method Based on RPC Model for Polarimetric SAR Data. *Remote Sens.* **2023**, *15*, 1909. [CrossRef]
3. Shiroma, G.H.X.; Lavalle, M.; Buckley, S.M. An Area-Based Projection Algorithm for SAR Radiometric Terrain Correction and Geocoding. *IEEE Trans. Geosci. Remote Sens.* **2022**, *60*, 5222723. [CrossRef]
4. Jiang, W.; Yu, A.; Dong, Z.; Wang, Q. Comparison and Analysis of Geometric Correction Models of Spaceborne SAR. *Sensors* **2016**, *16*, 973. [CrossRef]
5. Chen, X.; Sun, Q.; Hu, J. Generation of Complete SAR Geometric Distortion Maps Based on DEM and Neighbor Gradient Algorithm. *Appl. Sci.* **2018**, *8*, 2206. [CrossRef]
6. Kropatsch, W.G.; Strobl, D. The Generation of SAR Layover and Shadow Maps from Digital Elevation Models. *IEEE Trans. Geosci. Remote Sens.* **1990**, *28*, 98–107. [CrossRef]
7. Li, X.; Zhang, G.; Yin, C.; Wu, Y.; Shen, X. A Novel Shadow and Layover Segmentation Network for Multi-Angle SAR Images Fusion. *IEEE Access* **2022**, *10*, 117770–117781. [CrossRef]
8. Du, X.; Yang, Q.; Cai, B.; Liang, D. A New Method on Shadow and Layover Detection of InSAR. In Proceedings of the 2017 Sixth Asia-Pacific Conference on Antennas and Propagation (APCAP), Xi'an, China, 16–19 October 2017; pp. 1–3.
9. Farr, T.G.; Rosen, P.A.; Caro, E.; Crippen, R.; Duren, R.; Hensley, S.; Kobrick, M.; Paller, M.; Rodriguez, E.; Roth, L.; et al. The Shuttle Radar Topography Mission. *Rev. Geophys.* **2007**, *45*, 2005RG000183. [CrossRef]
10. Michael, A.; Bailey, B.; Hiroji, T.; Hato, M. The ASTER Global DEM. *Photogramm. Eng. Remote Sens.* **2010**, *76*, 344–348.
11. EORC, J. ALOS Global Digital Surface Model (DSM). *ALOS World* **2021**, *1*, 1–21.
12. Fahrland, E. *Copernicus DEM Product Handbook (v4.0)*; Airbus Defence and Space GmbH: Taufkirchen, Germany, 2022.
13. Rosario, J.; Shiroma, G.H.X.; Fattahi, H.; Meyer, F.; Jeong, S. Assessment of Terrain Dependence of Radiometric Terrain Corrected C-Band Sentinel-1 SAR Backscatter over Different Target Types. In Proceedings of the IGARSS 2023—2023 IEEE International Geoscience and Remote Sensing Symposium, Pasadena, CA, USA, 16–21 July 2023; pp. 4286–4289.
14. Filipponi, F. Sentinel-1 GRD Preprocessing Workflow. *Proceedings* **2019**, *18*, 11. [CrossRef]
15. CEOS. Analysis Ready Data for Land: Normalized Radar Backscatter 2021. Available online: https://ceos.org/ard/files/PFS/SAR/v1.1/CEOS-ARD_PFS_Synthetic_Aperture_Radar_v1.1.pdf (accessed on 15 November 2024).
16. Rüetschi, M.; Small, D.; Waser, L.T. Rapid Detection of Windthrows Using Sentinel-1 C-Band SAR Data. *Remote Sens.* **2019**, *11*, 115. [CrossRef]
17. Lazecky, M.; Wadhwa, S.; Mlcousek, M.; Sousa, J.J. Simple Method for Identification of Forest Windthrows from Sentinel-1 SAR Data Incorporating PCA. *Procedia Comput. Sci.* **2021**, *181*, 1154–1161. [CrossRef]
18. Dalponte, M.; Solano-Correa, Y.T.; Marinelli, D.; Liu, S.; Yokoya, N.; Gianelle, D. Detection of Forest Windthrows with Bitemporal COSMO-SkyMed and Sentinel-1 SAR Data. *Remote Sens. Environ.* **2023**, *297*, 113787. [CrossRef]
19. Feng, Y.; Negrón-Juárez, R.I.; Romps, D.M.; Chambers, J.Q. Amazon Windthrow Disturbances Are Likely to Increase with Storm Frequency under Global Warming. *Nat. Commun.* **2023**, *14*, 101. [CrossRef]
20. Giovannini, L.; Davolio, S.; Zaramella, M.; Zardi, D.; Borga, M. Multi-Model Convection-Resolving Simulations of the October 2018 Vaia Storm over Northeastern Italy. *Atmos. Res.* **2021**, *253*, 105455. [CrossRef]
21. Vaglio Laurin, G.; Puletti, N.; Tattoni, C.; Ferrara, C.; Pirotti, F. Estimated Biomass Loss Caused by the Vaia Windthrow in Northern Italy: Evaluation of Active and Passive Remote Sensing Options. *Remote Sens.* **2021**, *13*, 4924. [CrossRef]
22. LiDAR DTM—Modello Digitale Del Terreno—PAT 2014 / 2018 2020. Available online: https://data.europa.eu/data/datasets/p_tn-79c6cdf0-c73a-46ba-870c-704bf4e27ac3?locale=en (accessed on 15 November 2024).
23. LiDAR DSM First—Modello Digitale Della Superficie First Pulse—PAT 2014 / 2018 2020. Available online: http://data.europa.eu/88u/dataset/p_tn-9bb00ab2-8c9e-4afd-aac4-8b6caef3edc9 (accessed on 15 November 2024).
24. Dostalova, A.; Navacchi, C.; Greimeister-Pfeil, I.; Small, D.; Wagner, W. The Effects of Radiometric Terrain Flattening on SAR-Based Forest Mapping and Classification. *Remote Sens. Lett.* **2022**, *13*, 855–864. [CrossRef]
25. Xiang, Y.; Jiao, N.; Liu, R.; Wang, F.; You, H.; Qiu, X.; Fu, K. A Geometry-Aware Registration Algorithm for Multiview High-Resolution SAR Images. *IEEE Trans. Geosci. Remote Sens.* **2022**, *60*, 1–18. [CrossRef]
26. Small, D. Flattening Gamma: Radiometric Terrain Correction for SAR Imagery. *IEEE Trans. Geosci. Remote Sens.* **2011**, *49*, 3081–3093. [CrossRef]
27. *SAR Geocoding: Data and Systems*; Schreier, G., Ed.; Wichmann: Karlsruhe, Germany, 1993; ISBN 978-3-87907-247-7.

28. R Core Team. *R: A Language and Environment for Statistical Computing*; R Foundation for Statistical Computing: Vienna, Austria, 2022.
29. Bovolo, F.; Bruzzone, L. A Detail-Preserving Scale-Driven Approach to Change Detection in Multitemporal SAR Images. *IEEE Trans. Geosci. Remote Sens.* **2005**, *43*, 2963–2972. [CrossRef]
30. Marin, C.; Bovolo, F.; Bruzzone, L. Building Change Detection in Multitemporal Very High Resolution SAR Images. *IEEE Trans. Geosci. Remote Sens.* **2015**, *53*, 2664–2682. [CrossRef]
31. Han, K.; Zeng, Q.; Wang, H.; Jiao, J. Comparison of Sar Image Geometric Correction Based on Multi-Resolution DEMS. In Proceedings of the IGARSS 2018—2018 IEEE International Geoscience and Remote Sensing Symposium, Valencia, Spain, 22–27 July 2018; pp. 581–584.
32. Lee, K.Y.; Byun, Y.G.; Kim, Y.S. Accuracy Evaluation of Terrain Correction of High Resolution SAR Imagery with the Quality of DEM. *K. J. Geomat.* **2012**, *30*, 519–528. [CrossRef]
33. Schlund, M.; Baron, D.; Magdon, P.; Erasmi, S. Canopy Penetration Depth Estimation with TanDEM-X and Its Compensation in Temperate Forests. *ISPRS J. Photogramm. Remote Sens.* **2019**, *147*, 232–241. [CrossRef]
34. Chen, H.; Cloude, S.R.; Goodenough, D.G. Forest Canopy Height Estimation Using Tandem-X Coherence Data. *IEEE J. Sel. Top. Appl. Earth Obs. Remote Sens.* **2016**, *9*, 3177–3188. [CrossRef]
35. Chai, L.T.; Wong, C.J.; James, D.; Loh, H.Y.; Liew, J.J.F.; Wong, W.V.C.; Phua, M.H. Vertical Accuracy Comparison of Multi-Source Digital Elevation Model (DEM) with Airborne Light Detection and Ranging (LiDAR). *IOP Conf. Ser. Earth Environ. Sci.* **2022**, *1053*, 012025. [CrossRef]
36. Goyal, S.K.; Seyfried, M.S.; O'Neill, P.E. Effect of Digital Elevation Model Resolution on Topographic Correction of Airborne SAR. *Int. J. Remote Sens.* **1998**, *19*, 3075–3096. [CrossRef]
37. Truckenbrodt, J.; Freemantle, T.; Williams, C.; Jones, T.; Small, D.; Dubois, C.; Thiel, C.; Rossi, C.; Syriou, A.; Giuliani, G. Towards Sentinel-1 SAR Analysis-Ready Data: A Best Practices Assessment on Preparing Backscatter Data for the Cube. *Data* **2019**, *4*, 93. [CrossRef]